Journal Pre-proof

Revealing insights into the correlations between structure and performance of CrO_X monometallic oxide for Hg^0 capture

Dong Ye, Shujie Gao, Zhichang Jiang, Xiaoxiang Wang, Yaolin Wang, Hui Liu, Haining Wang

PII: S1743-9671(23)00014-4

DOI: https://doi.org/10.1016/j.joei.2023.101185

Reference: JOEI 101185

To appear in: *Journal of the Energy Institute*

Received Date: 29 November 2022

Revised Date: 4 January 2023

Accepted Date: 9 January 2023

Please cite this article as: D. Ye, S. Gao, Z. Jiang, X. Wang, Y. Wang, H. Liu, H. Wang, Revealing insights into the correlations between structure and performance of CrO_X monometallic oxide for Hg^0 capture, *Journal of the Energy Institute* (2023), doi: https://doi.org/10.1016/j.joei.2023.101185.

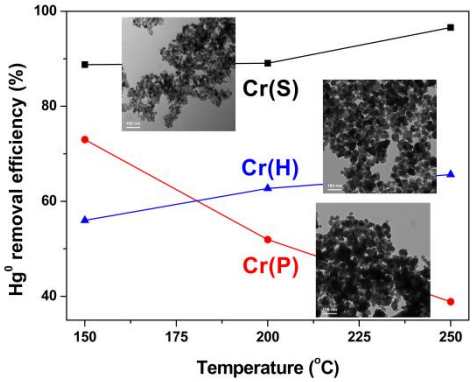

Revealing insights into the correlations between structure and performance of CrO_x monometallic oxide for Hg^0 capture

Dong Ye[a]*, Shujie Gao[a], Zhichang Jiang[a], Xiaoxiang Wang[b], Yaolin Wang[c], Hui Liu[a], Haining Wang[a]*

[a]*College of Quality & Safety Engineering, China Jiliang University, Hangzhou, 310018, China*

[b]*Key Laboratory of Biomass Chemical Engineering of Ministry of Education, Institute of Industrial Ecology and Environment, College of Chemical and Biological Engineering, Zhejiang University, Hangzhou, 310027, China*

[c]*Department of Electrical Engineering and Electronics, University of Liverpool, Liverpool L69 3GJ, UK*

*Corresponding author: Dong Ye

Tel: +86 571 86872370

E-mail: Richard32@126.com

*Corresponding author: Haining Wang

Tel: +86 571 86872370

E-mail: whnfyy@163.com

Nomenclature

M	mass of the tested sample, g
F	total flow rate of the reactant gas, ml/min
t	capture time of Hg^0, min
q	Hg^0 capture capacity, μg/g
η	Hg^0 removal efficiency
A_{out}	outlet concentration of Hg^0, $\mu g/m^3$
A_{in}	inlet concentration of Hg^0, $\mu g/m^3$
B	potential mass transfer index, mg/g
b	adsorbate-adsorbent affinity parameter, g×h/mg
$[k_La]_f$	external mass transfer factor, h^{-1}
$[k_La]_g$	global mass transfer factor, h^{-1}
$[k_La]_d$	internal mass transfer factor, h^{-1}
k_1	pseudo-first-order rate constant, min^{-1}
k_2	pseudo-second-order rate constant, min^{-1}
q_e	equilibrium Hg^0 capture capacity, μg/g
k_p	intraparticle diffusion coefficient, $\mu g/(g*min^{1/2})$
c	constant related to the boundary conditions, μg/g
α	initial adsorption rate constant, $\mu g/(g*min^{1/2})$
β	desorption rate constant, g/μg

Abstract

This study explored the impacts of the synthesis methods on the Hg^0 elimination ability of CrO_x adsorbents. In the sample series, the adsorbent prepared using the sol-gel method (labeled as Cr(S)) presented the best Hg^0 capture performance; its Hg^0 removal efficiency stayed above 88% at 150 and 200 ^oC and even rose to ~97% at 250 ^oC in the entire 5-hour Hg^0 capture process. The presence of bountiful surface acid sites aided the sufficient adsorption of Hg^0 and an enhancement in the oxidizability primarily accelerated the subsequent Hg^0 oxidation step, which constituted the central reason for the satisfactory Hg^0 capture capability of Cr(S). The Mars-Maessen mechanism assisted in understanding the Hg^0 capture process over Cr(S), in which chemisorption was dominant with Cr^{6+} and O_α serving as the active sites and HgO formed as the final oxidation product.

Keywords: CrO_x, preparation methods, acid sites, oxidizability, Hg^0 elimination ability.

1. Introduction

Mercury, one of the typical heavy metals in exhausted gas, has gained considerable attention throughout the world owing to this species' high toxicity and bioaccumulation [1]. The agreement of Minamata Convention on Mercury means that global efforts must be made to reduce the emission of mercury so as to protect the environment and human health [2]. It is understood that mercury in exhausted flue gas always appears as oxidized mercury (Hg^{2+}), particulate-bound mercury (Hg^{p}), and elemental mercury (Hg^{0}) [3]. Despite the comparably high removal efficiency of the former two species by the existing wet flue gas desulfurization (WFGD) systems and dust control devices, the capture of Hg^{0} is still the main barrier to the effective reduction of mercury emission because of its low solubility and high volatility [4].

Thanks to its satisfactory Hg^{0} elimination efficiency and low operation cost, the adsorbent injection technique is gaining increasing popularity in engineering. As a predominant issue, designing an adsorbent with superior reactivity primarily contributes to the high Hg^{0} removal efficiency of the entire system [5, 6]. In light of the fact that the Hg^{0} capture process is a dual-site reaction, combining a novel acidity and a strong oxidizablity could ensure the sufficient adsorption and oxidation of Hg^{0}, thereby allowing a relatively high Hg^{0} capture capacity obtained [7].

CrO_x, which is famous for its extraordinarily strong acidity and abundance of reactive surface oxygen vacancies, appears to be suitable for Hg^{0} removal [8]. Given that CrO_x was used as a dopant or directly taken as an adsorbent, the material was found to be active for Hg^{0} capture. Moreover, a relatively high stability under acidic or neutral conditions demonstrates that CrO_x can almost be regarded as an environmental-benign material [7]. These findings confirm that with proper modification, CrO_x would present certain potential for Hg^{0} elimination in practical engineering cases.

It is understood that the preparation method is a predominant factor to influence the adsorbent physico-chemical features [9]. This is because different chemicals and

experimental conditions used would cause the variations in the crystal growth and the active species' contents, distributions and existing forms [10]. That is to say, by selecting the appropriate synthesis method, it seems that the previously indicated qualities of the adsorbent can be optimized so that its maximum Hg^0 removal ability can be ultimately achieved. In this study, CrO_x adsorbents were synthesized using the conventional precipitation, sol-gel, and hydrothermal methods. The related samples are successively labeled as Cr(P), Cr(S), and Cr(H). With their Hg^0 elimination ability evaluated, some characterizations including transmission electron microscope (TEM), X-ray diffraction (XRD), N_2 adsorption, Raman, NH_3-temperature programmed desorption (NH_3-TPD), H_2-temperature programmed reduction (H_2-TPR), X-ray photoelectron spectroscopy (XPS), and Hg^0-temperature programmed desorption (Hg^0-TPD) were conducted to discover the mechanistic aspects of the adsorbents, along with their structural and chemical qualities.

2. Experimental

2.1 Adsorbent synthesis

Cr(S): $Cr(NO_3)_3 \cdot 9H_2O$ was used as the precursor and citric acid was selected as the capping ligand. $Cr(NO_3)_3 \cdot 9H_2O$ and citric acid at molar ratio of 1/2 were dissolved in deionized water. The resultant dark-green solution was aged at 80 ^oC under the atmosphere of air in an oven. 16 h later, the obtained power was annealed at 500 ^oC in air for 5 h.

Cr(P): $Cr(NO_3)_3 \cdot 9H_2O$, the precursor, was dissolved in deionized water to form transparent solution, which was subsequently dropwise added into 30 ml diluted ammonia solution (wt: 12.5~14%). After filtration, the paste was rinsed with 500 mL deionized water five times. At last, the resulted product was dried at 80 ^oC in air for 16 h and annealed at 500 ^oC for 5 h.

Cr(H): 20 mL 1mol/L chromic nitrate solution was mixed with 50 mL 2 mol/L sodium hydroxide solution. After the hydrothermal process at 80 ^oC for 9 hours, the

cyan-colored product was rinsed with diluted acetic acid solution (pH=5) and deionzed water several times until the pH value of the supernatant reaches 7. In the end, the greenish paste was dried at 80 °C in air for 16 h and annealed at 500 °C for 5 h.

2.2 Adsorbent testing

A fixed-bed micro-reactor was employed to test the adsorbent Hg^0 removal performance in accordance with our previous studies [7]. Hg^0 vapor was generated through a mercury permeation tube immersed in a water bath at 35 °C. The composition of the reactant gas (400 mL/min) was 200 μg/m^3 + 5% O_2 + balance N_2. In each test, 0.1 g sample was used. Hg^0 signal was monitored on an online mercury analyzer (RA-915M, LUMEX Ltd., Russia). Hg^0 capture capacity and Hg^0 removal efficiency were selected to evaluate the Hg^0 elimination ability of the adsorbent, which can be determined as follows:

$$q = \frac{1}{M}\int_{t_1}^{t_2}(A_{in} - A_{out})\,Fdt \quad (1)$$

$$\eta = 100\% \times \frac{A_{in} - A_{out}}{A_{in}} \quad (2)$$

2.3 Adsorbent characterization

XRD, N_2 adsorption, TEM, and Raman techniques were employed to characterize the textural features of the adsorbents. NH_3-TPD, H_2-TPD, and XPS characterizations were carried out to investigate the adsorbent acid and redox qualities. Hg^0-TPD experiment was conducted to uncover the final product of the Hg^0 capture process so that the corresponding mechanisms could be illustrated. The detailed information on these characterizations are presented in the Supporting Information.

3. Results and discussions

3.1 Hg^0 capture ability

Fig. 1 depicts the Hg^0 capture ability of the three investigated samples. It can be seen that an ongoing reaction process always leads to the increase in the outlet concentration of Hg^0. In the sample series, Cr(S) has a rather strong ability to capture Hg^0; the related Hg^0 removal efficiency after 5 hours stays above 88% at 150, 200, and 250 ^oC. Notably, as the reaction temperature is raised, an enhancement in the Hg^0 elimination performance of Cr(S) takes place; at 250 ^oC, ~97% Hg^0 removal efficiency is reached during the 5-hour test period. As is presented in Table S1, substantial parts of the reported adsorbents are just proven to be active in the flue gas with a relatively low Hg^0 concentration (tens of $\mu g\ m^{-3}$). Considering the variable flue gas conditions in industrial sources, whether or not Hg^0 can also be effectively captured from the flue gas with an elevated Hg^0 content (hundreds of $\mu g\ m^{-3}$) is still unclear. But such knowledge is crucial to the practical application of the adsorbents. In our case, it appears that this issue can be somehow addressed.

Similar phenomenon can be observed for Cr(H) that the increase of the temperature boosts the proceeding of the Hg^0 capture reaction. Instead, with rising the temperature, the Hg^0 capture ability of Cr(P) exhibits a trend of decline. Moreover, Hg^0 removal efficiency of Cr(H) after 5 hours outstrips that of Cr(P) at 200 ^oC; further rising the temperature to 250 ^oC, the gap of the Hg^0 removal efficiency between Cr(H) and Cr(P) becomes great. This should be ascribed to the variations in the structural and chemical features of these three samples, which would be illustrated using some characterizations, including XRD, Raman, and so on.

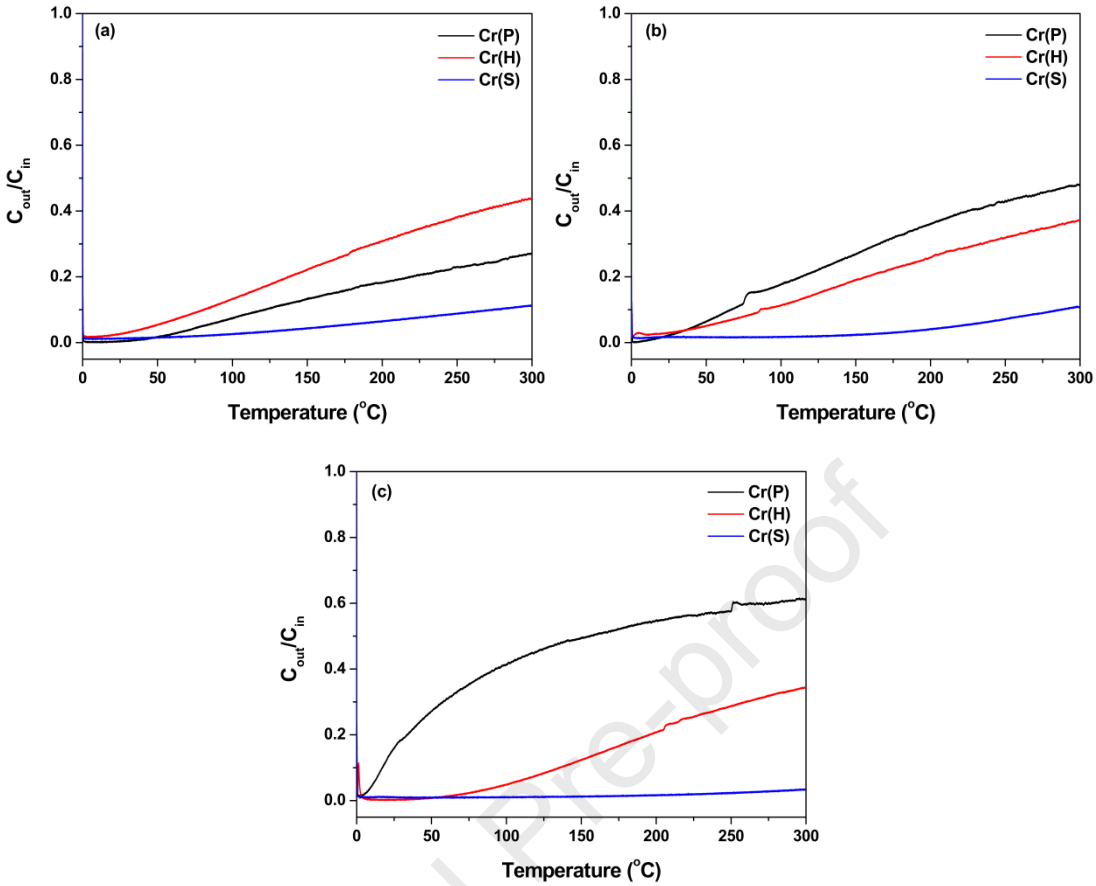

Fig. 1 Hg^0 breakthrough profiles of the serial samples: (a) 150 °C, (b) 200 °C, and (c) 250 °C.

3.2 Structural and textural features

TEM images shows the micro-features of the three Cr oxides (Fig. 2). In the case of the sample prepared using the sol-gel method, only irregular particles with the size of ~10 nm can be observed. While for the other two samples, it appears that the diameter of the irregular particles rises, which is indicative of an increase in the adsorbent crystallinity and grain size [7]. That would lead to the different structural and chemical qualities of the adsorbents, thus varying their Hg^0 elimination abilities.

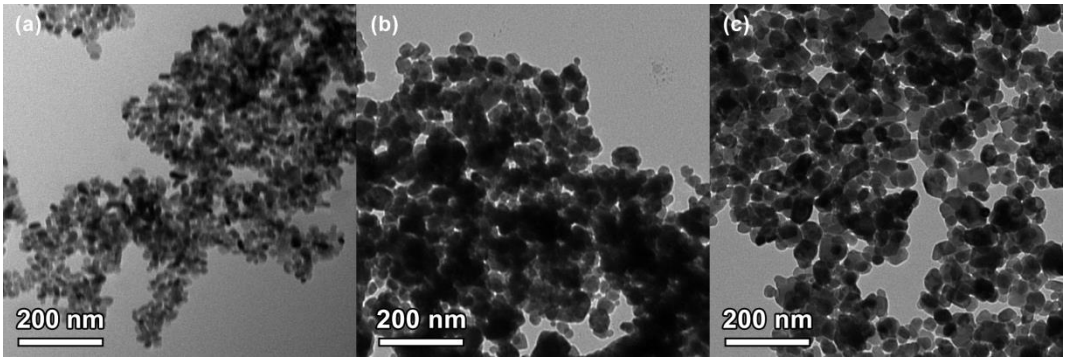

Fig. 2 TEM images of (a) Cr(S), (b) Cr(P), and (c) Cr(H).

The wide-angle XRD profiles of Cr(S), Cr(P), and Cr(H) are illustrated in Fig. 3(a). For each sample, only the peaks identical to those of Cr_2O_3 phase are present. Compared with Cr(S), an increase in the peak intensity seems to take place for the other two samples. This phenomenon means that by employing the sol-gel method, the growth of the crystals might be somehow interfered, which would allow the adsorbent grain size to decrease and its specific surface area to potentially increase. The local structures of the adsorbent series were further investigated using Raman spectroscopy with the corresponding spectra presented in Fig. 3(b). The intense peak at ~551 cm^{-1} is identified as the metal-oxygen vibration of distorted octahedrally coordinated Cr species in crystalline Cr_2O_3 [11]. And the attribution of the other bands is summarized as follows. 309 and 353 cm^{-1}: $\delta(CrO_4)/(Cr'O_3)$; 606 cm^{-1}: $\nu_s(Cr'OCr'')$; 702 cm^{-1}: $\nu_{as}(Cr'OCr'')$; 824 cm^{-1}: $\nu_s(OCr''O)$; 992 cm^{-1}: $\nu_s(Cr''O_2)$; 1014 cm^{-1}: polymeric chromic species [11-13]. The presence of various chromic species reveals the fact that some defects might exist in these three samples, which would thus permit the appearance of Cr atoms with multi-oxidation numbers.

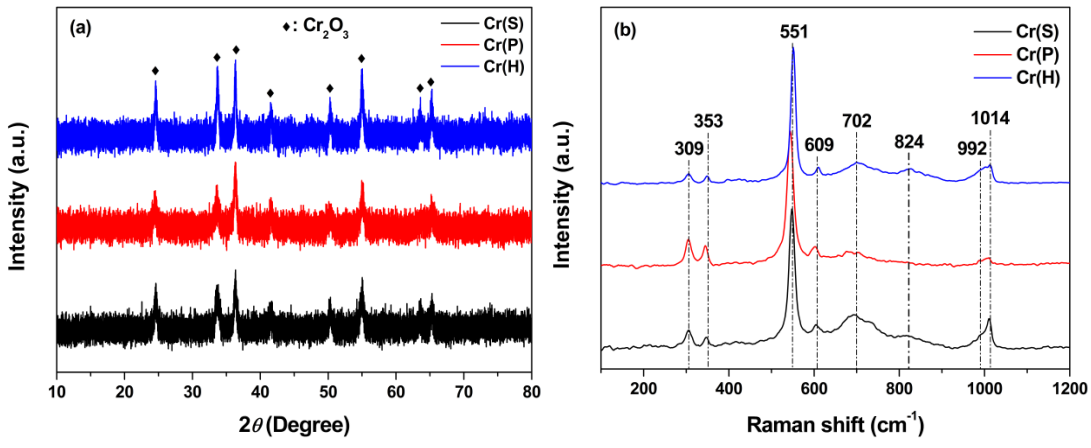

Fig. 3 (a) XRD patterns and (b) Raman spectra of Cr(S), Cr(P), and Cr(H).

N_2 adsorption-desorption isotherms of the serial CrO_x adsorbents are shown in Fig. 4(a). On the basis of the IUPAC classification, the isotherms of all the samples resembled closely with type IV isotherms [14]. In the case of Cr(P), the hysteresis loop presents typical H_2 type, which can be explained by the presence of the ink-bottle-shaped pore structure. In contrast, the isotherms of the other two samples in the high relative pressure range shift to H3 type, demonstrating the appearance of the slit-like pore structure. Fig. 4(b) clarifies the profiles of the adsorbent pore size distributions. For Cr(S), a sharp peak appears at *ca*. 18 nm, indicating a rather narrow pore size distribution. Instead, a comparably broad pore size distribution is obtained for Cr(P) and Cr(H). Data related to the adsorbent surface area, average pore diameter, and total pore volume are summarized in Table 1. In the sample series, Cr(S) exhibits the highest specific surface area, meaning that an increased number of active sites can be involved in Hg^0 elimination. That in part explains the best Hg^0 capture ability of Cr(S).

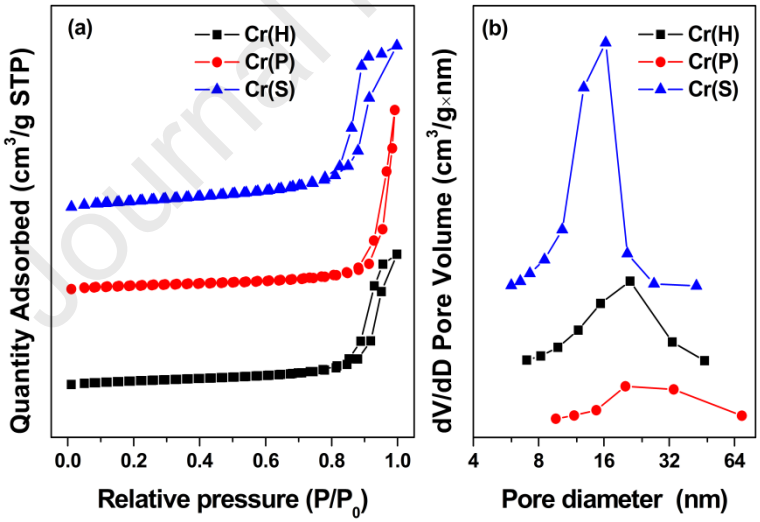

Fig. 4 (a) N_2 adsorption-desorption isotherms and (b) pore size distributions of the samples series.

Table 1 N_2 adsorption data of the samples series.

Samples	Surface area (m^2/g)	Pore size (nm)	Pore Volume (cm^3/g)
Cr(S)	57	15.0	0.28
Cr(P)	29	34.8	0.30
Cr(H)	32	20.1	0.22

3.3 Acid and redox properties

It is understood that Hg^0 is a basic molecule that has a great affinity to the adsorbent surface acid sites [15]. Therefore, the acid property appears to significantly affect the Hg^0 capture ability of an adsorbent. In order to clarify this feature, NH_3-TPD was conducted. Through curve-fitting, four sub-peaks are obtained with the temperature rising (Fig. 5(a)). Based on the literature, these four peaks can be successively identified as the physisorbed NH_3 and NH_3 linked to the weak, medium, and strong acid sites [16]. With calculating the adsorption quantity of NH_3 on these three types of acid sites (Fig. 5b), it can be estimated that the sample synthesized using the sol-gel method possesses the largest number of surface acid sites, which could assure the sufficient adsorption of Hg^0 and subsequently lead to the potentially elevated Hg^0 elimination performance.

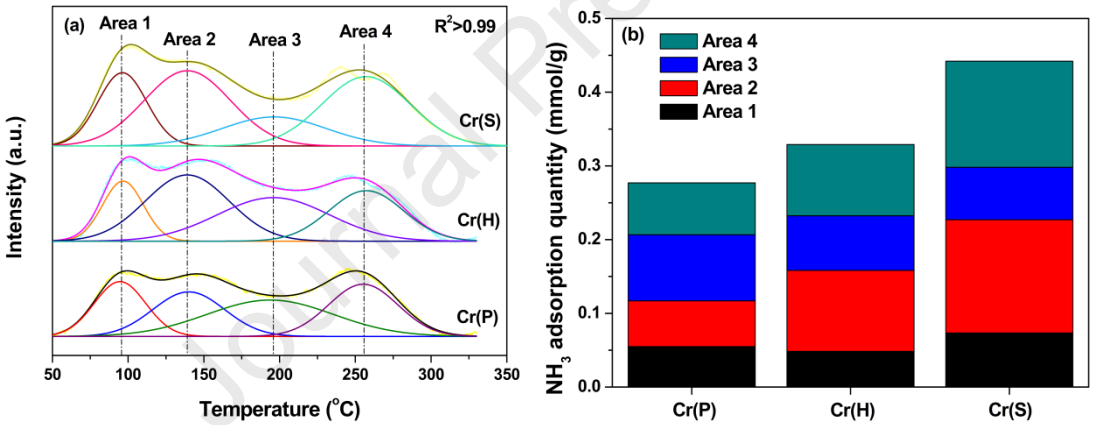

Fig. 5 (a) NH_3-TPD profile and (b) NH_3 adsorption quantity of the serial samples.

Fig. 6(a) shows the H_2-TPR profiles of the investigated adsorbents. According to the literature, the peaks with the temperature lower than 280 °C are closely related to the reduction of Cr^{6+} and surface capped oxygen species, which, in our previous study, were proven to be active in Hg^0 elimination reactions [7]. Thus, we calculated the areas of the peaks regarding to the reduction of these two species so as to estimate the amount of active species that can participate in Hg^0 capture. As is shown in Fig. 6(b), the quantity of Cr^{6+} and surface capped oxygen species follows the order of Cr(S) > Cr (P) > Cr(H), which partially contributes to the superior Hg^0 capture ability of Cr(S) in this sample series.

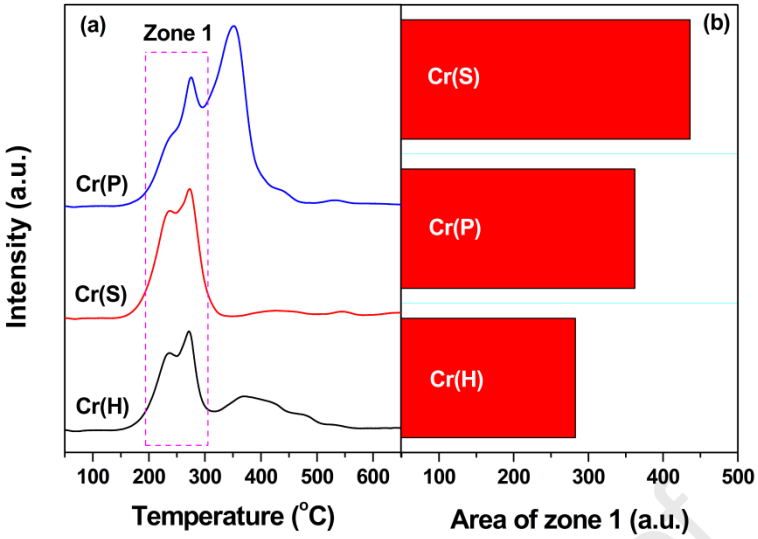

Fig. 6 H_2-TPR results of the sample series: (a) H_2-TPR profiles and (b) integrated area of zone 1.

Cr and O atom information of the serial adsorbents were determined via utilizing the XPS technique. As is presented in Fig. 7(a), sub-peaks at ~578.4, 576.2, and 575.2 eV can be successfully identified as Cr^{6+}, Cr^{3+}, and Cr^{2+} [8]. This result reveals that Cr cations in multi-valance states are present in these three samples, which is somehow in accordance with the Raman spectra in Fig. 3(b). Meanwhile, the curve-fitting of the O 1s spectra indicates the presence of various oxygen species. The appearance of lattice oxygen (O_β) and chemisorbed oxygen (O_α) gives rise to the sub-peaks at ~531.1 and 529.8 eV, respectively (Fig. 7(b)) [17]. The relative contents of Cr^{6+} and O_α species are estimated on the basis of the corresponding spectra and follow the order of Cr(S) > Cr(P) > Cr(H) (Table 2), which, to some extent, is consistent with the H_2-TPR spectra in Fig. 6 that Cr(S) has a comparably strong oxidative ability and in part explains its best Hg^0 elimination performance.

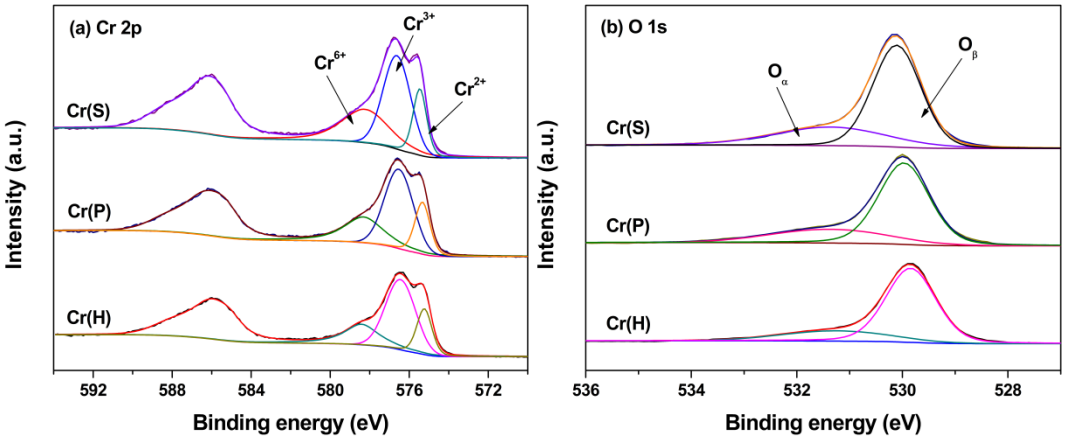

Fig. 7 XPS spectra: (a) Cr 2p and (b) O 1s.

Table 2 XPS data of Cr(H), Cr(S), and Cr(P).

Sample	Cr^{6+} (%)	O_α (%)
Cr(S)	35.1	31.0
Cr(H)	26.4	21.7
Cr(P)	30.3	26.3

3.4 Mechanisms

On the basis of the afore-mentioned results, selecting the Cr(S) sample to study the Hg^0 capture mechanisms seems to be reasonable owing to its best Hg^0 elimination ability in the adsorbent series. Moreover, this result can assist in digging out the predominant factors in the Hg^0 capture cycles and hence achieving the goal of the practical applications of the adsorbents.

According to the literature, the mass-transfer process, which consists of an external mass transfer, an internal mass transfer and a global mass transfer, is believed to be a crucial step in the Hg^0 removal reactions because of its considerable impacts on the Hg^0 removal efficiency of an adsorbent. The following four equations can depict these three stages [18]:

$$ln\left(\frac{A_{in}}{A_{out}}\right) = [k_L a]_f \times t \quad (3)$$

$$[k_L a]_f = [k_L a]_g \times e^{-b \times ln(q)} \quad (4)$$

$$[k_L a]_d = [k_L a]_g - [k_L a]_f \quad (5)$$

$$ln(q) = B + \frac{1}{b} \times ln(t) \quad (6)$$

Given the linear fitting of the experimental data, it appears reasonable to employ the *B* and *b* parameters to reflect the mass transfer potential during Hg^0 elimination and the affinity between Hg^0-adsorbent (Fig. 8(a) and Table S2). In the initial 120 min, the absolute values of $[k_L a]_f$, $[k_L a]_d$, and $[k_L a]_g$ drop sharply (Fig. 8(b), (c), and (d)). As the Hg^0 capture process goes on, negligible changes of these three parameters are presented, demonstrating that the mass-transfer process just play certain roles in the initial Hg^0 capture stage.

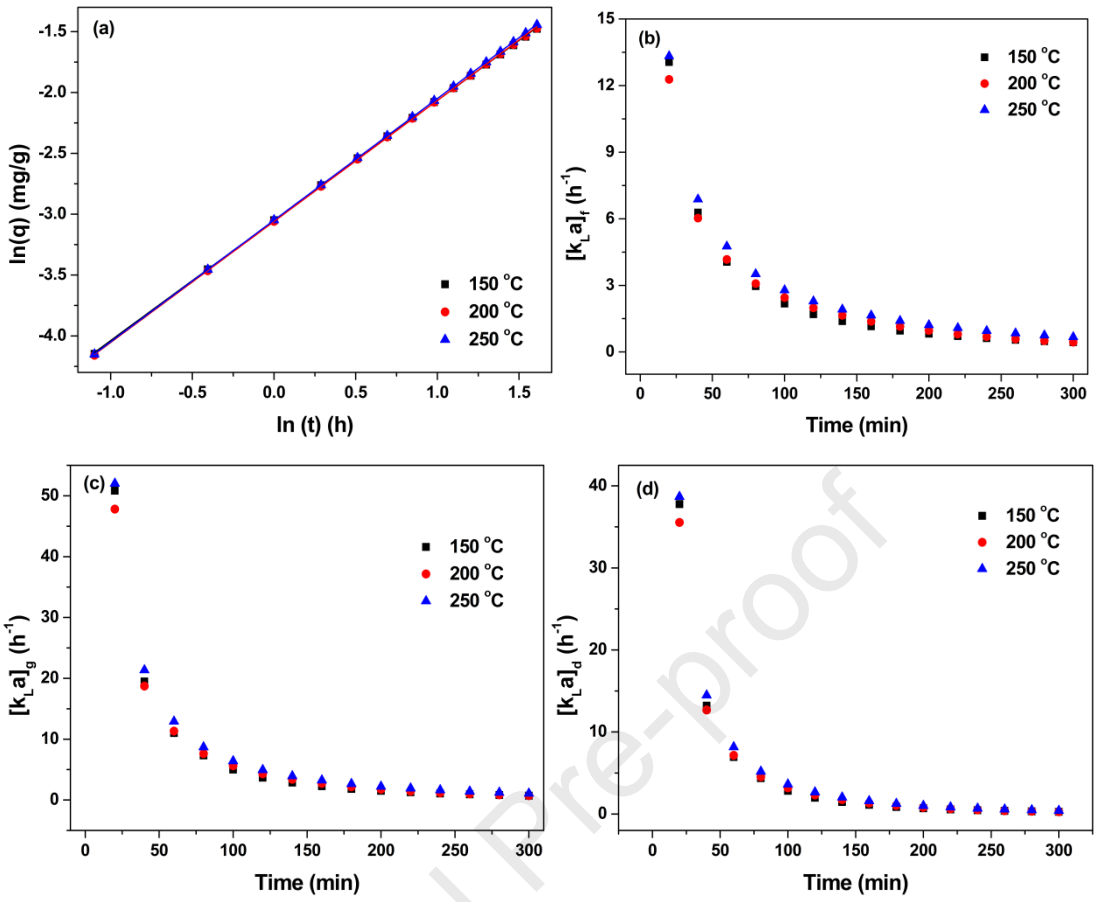

Fig. 8 (a) Linear-fitting analysis, (b) $[k_La]_f$, (c) $[k_La]_g$, and (d) $[k_La]_d$ profiles.

Hg^0 capture kinetics of the adsorbents were depicted through the curving-fitting of the pseudo-first order (eq. (7)), Webber-Morris (eq. (9)), pseudo-second order (eq. (8)), and Elovich (eq. (10)) models to the experimental data [19]. As is illustrated in Fig. 9, adsorbent accumulative Hg^0 capture capacity increases almost linearly as the reaction process goes on. The correlation coefficient (R^2) in Table 3 demonstrates the fact that the Hg^0 elimination process over Cr(S) adsorbent can be well explained by the pseudo-first order, pseudo-second order, and Elovich models; chemisorption is dominant in the entire Hg^0 removal process, in which the initial capture process hold crucial roles to play [20, 21]. This result, to some extent, is in accordance with the conclusions arrived at in Fig. 8.

$$\frac{dq_t}{dt} = k_1(q_e - q_t) \quad (7)$$

$$\frac{dq_t}{dt} = k_2(q_e - q_t)^2 \quad (8)$$

$$q_t = k_p t^{1/2} + c \quad (9)$$

$$q_t = \frac{1}{\beta} ln(t + \alpha\beta) - \frac{1}{\beta} \ln(\frac{1}{\alpha\beta}) \quad (10)$$

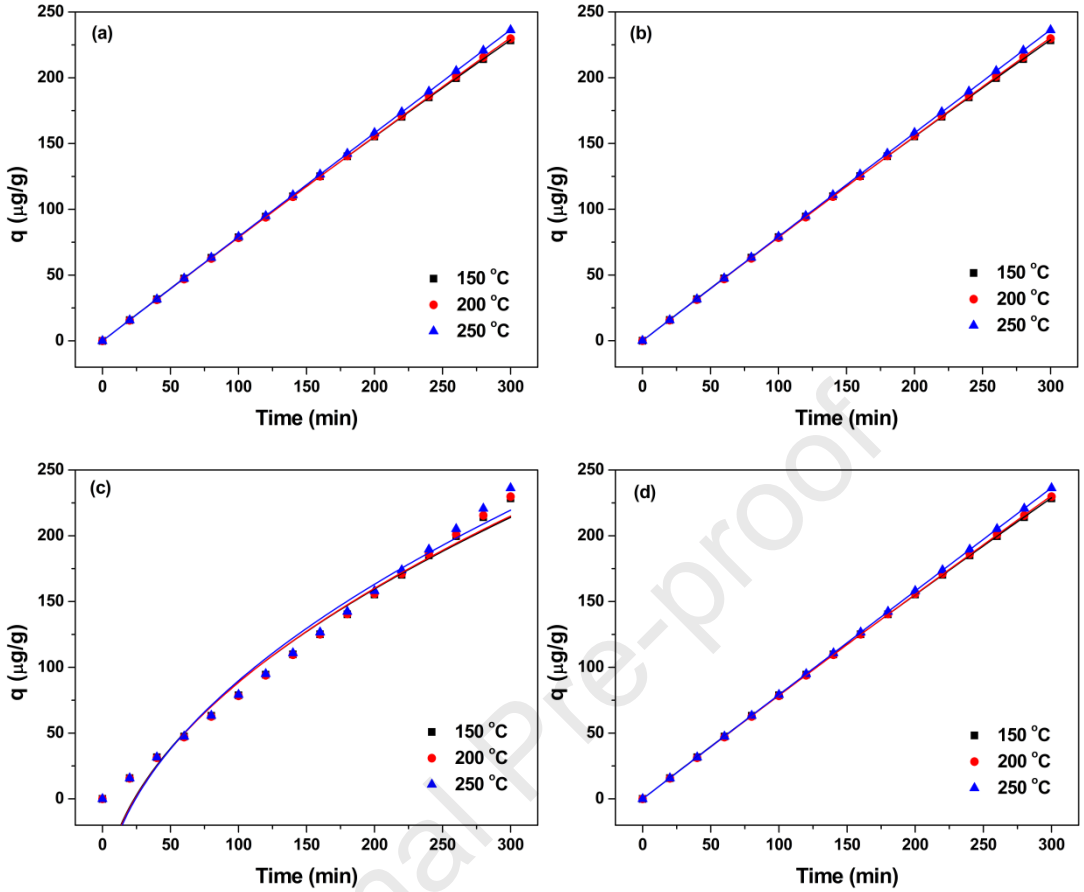

Fig. 9 Kinetic study of Hg^0 capture over Cr(S): (a) pseudo-first-order model, (b) pseudo-second-order model, (c) Webber-Morris model, and (d) Elovich model.

Table 3 Correlation coefficient (R^2) of curve-fitting.

Temperature	Correlation coefficient (R^2)			
(°C)	Pseudo-first-order	Pseudo-second-order	Weber-Morris	Elovich
150 °C	0.99999	0.99999	0.97693	0.99999
200 °C	0.99997	0.99997	0.97573	0.99997
250 °C	1	1	0.97320	1

Variations in the surface atom valence states of the adsorbents after the exposure in Hg^0-containing flue gas were explored using the XPS method so that the possible Hg^0 capture mechanisms can be summarized. In comparison with fresh Cr(S), it appears that the contents of Cr^{6+} and O_α exhibit a trend of decline (Fig. 10(a), (b) and Table 4), revealing the fact that the Hg^0 elimination process proceeds on Cr^{6+} and O_α sites. And on the basis of the Hg 4f spectra and the Hg^0-TPD profile in Fig. 10(c), it

can be estimated that the main form of the captured mercury species is HgO [22, 23]. Consequently, the Mars-Maessen mechanism seems to be able to explain the Hg^0 elimination pathway over Cr(S). The serial elementary reactions are shown below:

$$Hg^0(g) \rightarrow Hg^0(ads) \quad (11)$$

$$Hg^0(ads) + CrO_x \rightarrow Hg - O \equiv CrO_{x-1} \quad (12)$$

$$Hg - O \equiv CrO_{x-1} \rightarrow HgO(ads) + CrO_{x-1} \quad (13)$$

$$CrO_{x-1} + {}^1/_2\, O_2 \rightarrow CrO_x \quad (14)$$

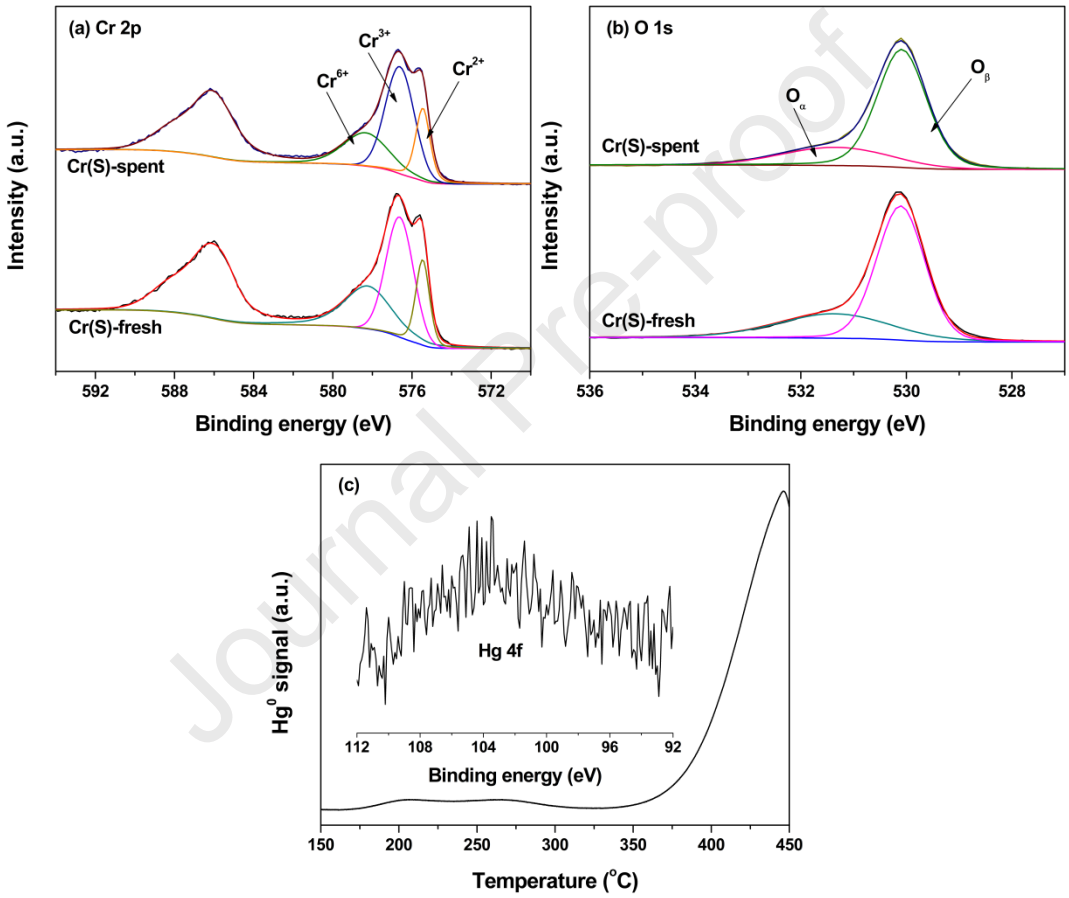

Fig. 10 XPS spectra of fresh and spent samples: (a) Cr 2p, (b) O 1s, (c) Hg 4f, and Hg^0-TPD profile (inset).

Table 4 XPS data of fresh and spent samples.

Sample	Cr^{6+} (%)	O_α (%)
Cr(S)-fresh	35.1	31.0
Cr(S)-spent	20.2	23.7

3.5 Discussions

According to the Hg^0 capture mechanisms, it appears that the acidity quality holds a crucial role to play in the adsorbent Hg^0 removal efficiency, for the adsorption of Hg^0 onto the surface acid sites constitutes the first step. Based on the NH_3-TPD results in Fig. 5, it can be seen that numerous acid sites are present on the surface of Cr(S), which allows the efficient adsorption of Hg^0 and thus supplies enough reactant for the subsequent oxidation step, in which adsorbent redox properties are mainly involved. H_2-TPR results in Fig. 6 and XPS data in Fig. 7 demonstrate that the presence of bountiful Cr^{6+} and surface capped oxygen, the highly reactive species, can be responsible for the accelerated oxidation of the adsorbed Hg^0. Notably, the optimized textural feature might be beneficial for the diffusion of the reactant, which consequently contributes to a high Hg^0 removal efficiency of Cr(S) at 150 ºC . For Cr(P), even if just limited amount of acid sites can be utilized to adsorb Hg^0, yet a rather high content of Cr^{6+} and surface capped oxygen would ensure the efficient oxidation of the adsorbed Hg^0. In other words, a comparably strong oxidizability can somehow overcome the drawbacks of the lower acidity, thus causing an increased amount of Hg^0 captured on Cr(P) compared to Cr(H).

As the reaction temperature is raised to 200 ºC or higher, the strong acid sites seem to be the dominant sites for the adsorption of Hg^0. For Cr(S) and Cr(H), even though the number of acid sites participating in adsorbing Hg^0 decreases, yet the presence of bountiful strong acid sites might still allow certain parts of Hg^0 adsorbed. Moreover, the subsequent oxidation step of Hg^0 would be exponentially accelerated, which still makes a considerable amount of Hg^0 effectively captured on the adsorbent surface as HgO [24, 25]. That is to say, the positive impact of the enhanced oxidation of Hg^0 might overcome the problem of the weakened adsorption of Hg^0 with the temperature ramped, hence leading to an enhancement in the Hg^0 elimination ability of these two samples. In contrast, a relatively low number of strong acid sites are present on Cr(P) surface, meaning that only a small portion of Hg^0 can be adsorbed. Even though this sample has a high content of reactive Cr^{6+} and surface capped

oxygen, yet the lack of reactant restrains the proceeding of the reaction, thereby resulting in a weakened Hg^0 capture ability. In other words, the weak acidity might be the predominant barrier to obtaining an increased high-temperature Hg^0 removal efficiency for Cr(P).

Generally, the oxidizability primarily determines the Hg^0 elimination ability of an adsorbent in a low temperature region while the acidity is closely related to the adsorbent high-temperature Hg^0 removal efficiency. An enhancement in both of these two features could simultaneously boost the adsorption and oxidation of Hg^0 in the whole temperature range. Then the operation temperature window of the adsorbents would be broadened, facilitating an effective reduction of mercury emission.

4. Conclusions

In this study, we investigated the impacts of the synthesis methods on the Hg^0 elimination ability of CrO_x adsorbents. The following are the important conclusions arrived at:

(1) Compared with the adsorbents prepared using the precipitation and hydrothermal methods, Cr(S) exhibits a comparably satisfactory Hg^0 capture ability; in the entire 5-hour Hg^0 elimination cycle, its Hg^0 removal efficiency stays above 88% at 150 and 200 ^oC and even rises to ~97% at 250 ^oC.

(2) Cr(S) exhibits a comparably strong acidity, which aids the adsorption of Hg^0. Meanwhile, the presence of bountiful Cr^{6+} and O_α, the reactive species, accelerates the subsequent Hg^0 oxidation step. That primarily explains the best Hg^0 removal performance of Cr(S).

(3) The Mars-Maessen mechanism is able to describe the Hg^0 capture pathways over Cr(S), in which the chemisorption is predominant and the initial capture stage holds a central role to play.

CRediT authorship contribution statement

Dong Ye: Conceptualization, Validation, Writing - original draft, Writing - review & editing, supervision. **Xiaoxiang Wang:** Conceptualization. **Yaolin Wang:** Validation. **Shujie Gao:** Investigation. **Zhichang Jiang:** Investigation. **Hui Liu:** Writing - review & editing. **Haining Wang:** Writing - review & editing.

Declaration of Interest Statement

We declare no conflict of interest.

Acknowledgement

This work is supported by the Scientific Research Foundation in China Jiliang University and the Zhejiang Provincial Natural Science Foundation of China (No. LQ22E060003, LY22E040001).

Reference

[1] D. Jampaiah, A. Chalkidis, Y.M. Sabri, E.L.H. Mayes, B.M. Reddy, S.K. Bhargava, Catal. Today 324 (2019) 174-182.

[2] Y. Ma, T. Xu, J. Wang, Y. Shi, H. Wang, F. Xiong, H. Xu, Y. Ma, H. Zhang, Environ. Sci. Pollut. Res. 28 (2021) 16447-16457.

[3] A. Chalkidis, D. Jampaiah, M.H. Amin, P.G. Hartley, Y.M. Sabri, S.K. Bhargava, Langmuir 35 (2019) 8246-8256.

[4] A. Chalkidis, D. Jampaiah, P.G. Hartley, Y.M. Sabri, S.K. Bhargava, Fuel Process. Technol. 193 (2019) 317-327.

[5] C. He, B. Shen, F. Li, J. Hazard. Mater. 304 (2016) 10-17.

[6] Y. Ma, B. Mu, X. Zhang, D. Yuan, C. Ma, H. Xu, Z. Qu, S. Fang, Chem. Eng. J. 358 (2019) 1499-1506.

[7] D. Ye, X. Wang, R. Wang, Y. Hu, X. Liu, H. Liu, H. Wang, J. Environ. Chem. Eng. 10 (2022) 108252.

[8] D. Zhang, L.a. Hou, G. Chen, A. Zhang, F. Wang, R. Wang, C. Lill, Ind. Eng. Chem. Res. 57

(2018) 17245-17258.
[9] D. Ye, R. Wang, X. Wang, X. Liu, H. Liu, H. Wang, Appl. Surf. Sci.578 (2022).
[10] X. Gao, Y. Jiang, Y. Fu, Y. Zhong, Z. Luo, K. Cen, Catal. Commun. 11 (2010) 465-469.
[11] L.R. Mentasty, O.F. Gorriz, L.E. Cadus, Ind. Eng. Chem. Res. 38 (1999) 396-404.
[12] M.A. Vuurman, D.J. Stufkens, A. Oskam, J.A. Moulijn, F. Kapteijn, J. Mol. Catal. 60 (1990) 83-98.
[13] A. Oskam, D.J. Stufkens, M.A. Vuurman, J. Mol. Struct. 217 (1990) 325-334.
[14] Sing, K. Sw, Pure Appl. Chem. 57 (1985).
[15] S. Yang, Y. Guo, N. Yan, Z. Qu, J. Xie, C. Yang, J. Jia, J. Hazard. Mater. 186 (2011) 508-515.
[16] D. Ye, X. Wang, H. Liu, H. Wang, Mol. Catal. 496 (2020).
[17] J.C. Dupin, D. Gonbeau, P. Vinatier, A. Levasseur, Phys. Chem. Chem. Phys. 2 (2000) 1319-1324.
[18] M.A. Fulazzaky, M.H. Khamidun, R. Omar, Chem. Eng. J. 228 (2013) 1023-1029.
[19] L. Yang, J. Wu, B. Li, D. Liu, J. Energ. Inst. 94 (2021) 120-128.
[20] Y. Shi, S. Deng, H. Wang, J. Huang, Y. Li, F. Zhang, X. Shu, RSC Adv. 6 (2016) 15999-16009.
[21] D. Liu, Z. Zhang, F. Luo, J. Wu, Energ. Fuel. 34 (2020) 6851-6861.
[22] W. Ma, D. Ye, H. Wang, Appl. Sci. 12 (2022) 3769.
[23] J. Yang, Y. Zhao, J. Zhang, C. Zheng, Environ. Sci. Technol. 48 (2014) 14837-14843.
[24] S. Yang, N. Yan, Y. Guo, D. Wu, H. He, Z. Qu, J. Li, Q. Zhou, J. Jia, Environ. Sci. Technol. 45 (2011) 1540-1546.
[25] S. Yang, Y. Guo, N. Yan, D. Wu, H. He, Z. Qu, J. Jia, Ind. Eng. Chem. Res. 50 (2011) 9650-9656.

1. Over 88% Hg^0 removal efficiency is obtained for Cr(S) at 150, 200, and 250 °C.

2. The Mars-Maessen mechanism describes the Hg^0 capture pathways over Cr(S).

3. The Hg^0 capture reaction primarily proceeds on Cr^{6+} and O_α sites.

4. The enhanced acidity and oxidizability explain the best Hg^0 capture ability of Cr(S).

Declaration of interests

☑The authors declare that they have no known competing financial interests or personal relationships that could have appeared to influence the work reported in this paper.

☐The authors declare the following financial interests/personal relationships which may be considered as potential competing interests: